DOI: 10.1002/adma.200602792

Filling Fraction Dependent Properties of Inverse Opal Metallic Photonic Crystals**

By *Xindi Yu*, *Yun-Ju Lee*, *Robert Furstenberg*, *Jeffrey O. White*, and *Paul V. Braun**

Metallic photonic crystals, metal-based structures with periodicities on the scale of the wavelength of light, have attracted considerable attention due to the potential for new properties, including the possibility of a complete photonic bandgap with reduced structural constraints compared to purely dielectric photonic crystals,[1] unique optical absorption, thermally stimulated emission behavior,[2,3] and interesting plasmonic physics.[4] Photonic applications may include high-efficiency light sources,[5] chemical detection,[6] and photovoltaic energy conversion.[3] Other applications for 3D porous metals, so-called "metal foams", include acoustic damping, high strength to weight structures, catalytic materials, and battery electrodes.[7] The photonic properties of metallic inverse opal structures have been of significant interest because of the simplicity of fabrication and potential for large-area structures. However, in practice, experiments on metal inverse opals have been inconclusive,[8–10] presumably because of structural inhomogeneities due to synthetic limitations. In this work, we demonstrate an electrochemical approach for fabricating high-quality metal inverse opals with complete control over sample thickness, surface topography, and, for the first time, the structural openness (metal filling fraction (FF)). Optical measurements conclusively demonstrate that metal inverse opals modulate the absorption and thermal emission of the metal and that these effects only become 3D in nature at high degrees of structural openness.

Various metals, for example, Au, Ag, W, Pt, Pd, Co, Ni, and Zn,[10–14] have been formed into inverse opals. Here, Ni is selected because of its high reflectivity in the IR, temperature stability, and ease of electrochemical processing. Ni inverse opals are fabricated by using electrodeposition through a polystyrene (PS) opal template that was first deposited on a surface-treated Au film evaporated on a Si wafer. PS opals formed from microspheres ranging in diameter from 460 nm to 2.2 μm were used as templates; this paper focuses on metal inverse opals formed using 2.2 μm microspheres. Templated electrodeposition is observed in all systems; this range of microsphere diameters is not an upper or lower limit. The final thickness of the sample is regulated by controlling the total charge. After electrodeposition, the PS microspheres are removed with tetrahydrofuran, resulting in a Ni inverse opal. Although the electrodeposition is quite homogeneous, gradual thickness variations do occur over the sample surface. These variations turn out to be useful, as they generate regions of different number of layers and surface terminations over the same sample (Fig. 1). Scanning electron microscopy (SEM) reveals a direct correspondence between the color,

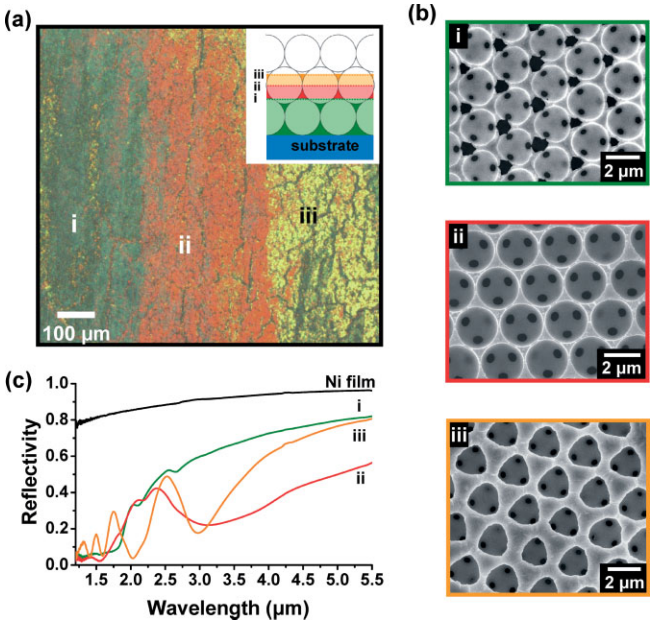

Figure 1. a) Optical microscopy image of the Ni inverse opal; the different surface topographies appear green (i), red (ii), and yellow (iii). Inset: Ni electrodeposition begins at the substrate and propagates upward. The top of the color bands correspond to the surface topography of three color regions observed under optical microscopy. b) SEM images of the three different surface topographies observed in (a). c) IR reflectance from the three color regions of an electrodeposited Ni film.

[*] Prof. P. V. Braun, X. Yu, Dr. Y.-J. Lee[+]
Department of Materials Science and Engineering
Frederick Seitz Materials Research Laboratory, Beckman Institute
University of Illinois at Urbana-Champaign
Urbana, IL 61801 (USA)
E-mail: pbraun@uiuc.edu
Dr. R. Furstenberg, Prof. J. O. White
Department of Physics, University of Illinois at Urbana-Champaign
Urbana, IL 61801 (USA)

[+] Present address: Sandia National Laboratories, PO Box 5800, MS 1082, Albuquerque, NM 87185, USA.

[**] The authors gratefully acknowledge helpful discussions with Xin Li, Dezhuan Han and Prof. Jian Zi of the Physics Department, Fudan University, Shanghai, China. This work is supported by the U.S. Department of Energy (DOE), Division of Materials Sciences, under Award No. DEFG02-91ER45439, through the Frederick Seitz Materials Research Laboratory at the Univ. of Illinois at Urbana-Champaign (UIUC) and the U.S. Army Research Laboratory and the U.S. Army Research Office under contract/grant number DAAD19-03-1-0227. Some experiments were performed in the Center for Microanalysis of Materials at UIUC, which is partially supported by the U.S. DOE under grant DEFG02-91-ER45439.

ADVANCED MATERIALS

green, red, or yellow, and the surface termination. As the color goes from green to red to yellow, the surface topography goes from shallow to deep bowl-like features to deep cavities with openings at the top, as expected for electrodeposition through a layer of colloidal particles.

The reflectivity of a Ni inverse opal with varying surface termination is collected at normal incidence using an Fourier transform IR (FTIR) microscope (Fig. 1c). The three different surface terminations exhibit very different properties, and agree qualitatively with previous observation on monolayer cavity structures.[15] Our data is consistent with a model where the optics are essentially due to a combination of Bragg plasmon and Mie plasmon interactions in the top layer of the structure.[15] Light does not directly penetrate into the structure due to the small skin depth of Ni (ca. 20 nm in near to mid IR) and the small size of the windows that connect the spherical cavities (SEM images in Fig. 1). Despite the fact that Bragg surface plasmon modes and TM Mie plasmon modes can have a strong field near the metal surface,[16] which can result in propagation of light through a porous metal film,[17] experimentally, we observe that plasmon-based propagation of light into our structure is minimal. This is probably because the geometry of the top layer is different from that of interior layers, limiting the overall plasmon-coupling efficiency.

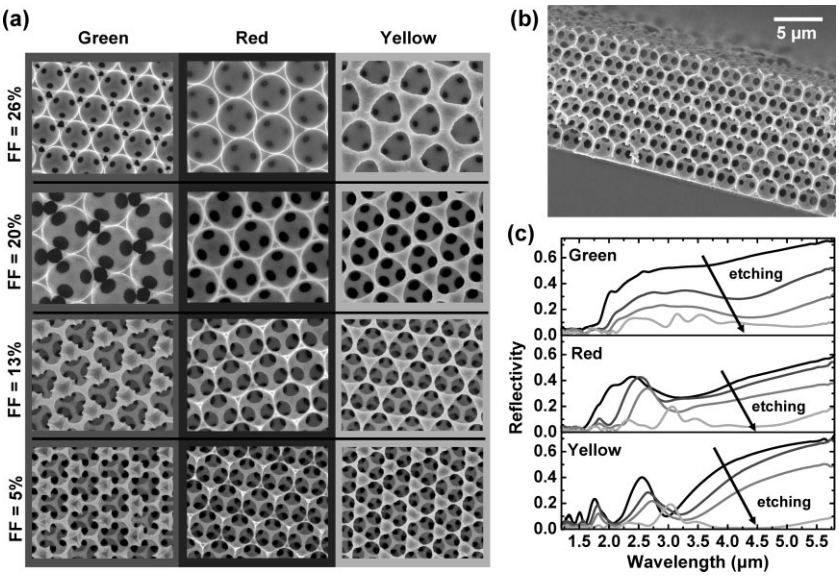

Figure 2. a) Top-view SEM images of Ni inverse opal of different surface topographies and structure openness. The four rows present nominal nickel FFs of 26 % (as deposited), 20 %, 13 %, and 5 % (maximum etching before structural collapse). The three columns correspond to the three different surface topographies described in Figure 1. b) SEM image of a Ni inverse opal cross section after etching (nickel FF = 13 %). Etching is uniform throughout the thickness of the structure. c) Reflectivity evolution as nickel FF reduces. Spectra are from the green, red, and yellow regions. For each color region, the traces correspond to FFs of 26 % (black), 20 % (dark grey), 13 % (grey), and 5 % (light grey), matching the SEM images in (a). All SEM images and reflective spectra are taken on the same four to five layer thick sample.

To increase the penetration depth of light, and thus explore the effect of 3D periodicity on the optical properties, the windows that interconnect the spherical cavities must be enlarged. This perhaps could be accomplished by depositing material around the PS opal prior to metal deposition, for example, Al_2O_3 by atomic layer deposition, which would increase the size of the windows and decrease the overall metal FF. However, Al_2O_3 would also deposit as an insulating layer on the substrate, preventing electrodeposition. Our preferred route rather is to homogeneously remove metal from the metal inverse opal by electroetching, a procedure commonly known as electropolishing, after removal of the colloidal template. Through control of the etching kinetics, the nickel inverse opals are uniformly etched through their entire thickness (Fig. 2b). The result of this etching can be structurally modeled as an increase in the diameter of the spherical cavities. The nickel FF after etching is determined by using SEM measurements.

The optical properties as a function of structural openness are determined by using successive electropolishing steps followed by measurements of optical properties. After each etching step, SEM images are collected to verify the amount of nickel removed. All spectra are collected from the same region of the sample. Figure 2 presents both the reflectivity evolution and SEM images of the three distinct surface topographies (three color areas) as the Ni volume fraction is reduced. The optical properties change dramatically as the interconnections between voids become larger and the nickel FF is reduced. As nickel is removed, the reflectivity generally decreases and the main features in the spectra shift to longer wavelengths. The most dramatic change is that the reflectivity spectra of three different color areas, which initially are quite different, become fairly similar. Light now propagates deep into the structure and surface effects become much less important. The optical properties of the structure are now truly 3D.

To determine the penetration depth of light into the Ni inverse opal, the reflectivity as a function of the number of layers and metal FF is measured from samples one to five layers thick (Fig. 3); each partially or completely formed layer is counted as one layer. Only the red color area is presented in Figure 3, the other two color areas exhibit similar behavior. In each graph, the four curves correspond to the four levels of etching exhibited in Figure 2a. Before etching, the spectra of all five samples are nearly identical, confirming that light is only interacting with the surface layer. As the structure opens up, spectra from samples of different thickness diverge. After the first etching step (dark-gray trace), the monolayer optical properties are different than the multilayer samples, but all multilayer samples are similar. By the final etching step (light-gray trace), the four- and five-layer samples are still similar,

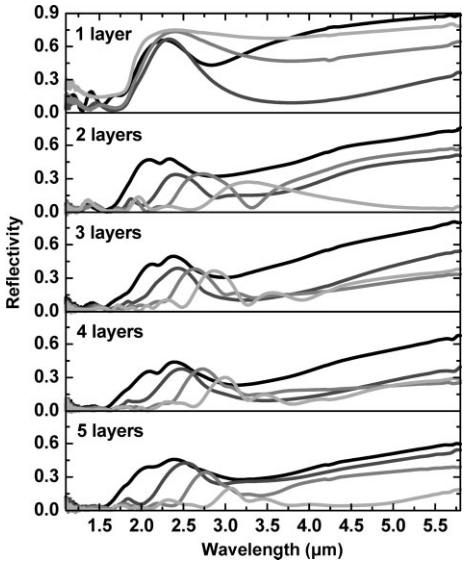

Figure 3. Ni inverse opal reflectivity as a function of thickness and FF. Reflectance spectra collected from one to five layer thick samples terminated with the "red" topography. Within each set of spectra, the grey scale scheme corresponds to the four different nickel FFs presented in Figure 2.

but the optical properties of the monolayer through three-layer samples are different. Qualitatively, this data indicates that light substantially penetrates three to four layers into the fully etched samples (ca. 5 % Ni by volume). The limited penetration depth is further confirmed by the less than 1 % transmission through a free-standing six-layer sample consisting of ca. 5 % Ni by volume, over all investigated wavelengths.

The thermal emission properties of metallic photonic crystals are of considerable interest.[2,5,18] Kirchoff's law states that emissivity (ε) and absorptance (a) of an object are equal for systems in thermal equilibrium. For the Ni inverse opals studied here, where transmission is negligible and Bragg scattering from the triangular pattern at the surface does not occur at wavelengths longer than ca. 1.9 μm for 2.2 μm spheres, in the sample normal direction, $\varepsilon = a = 1 - R$, with R being reflectivity. Emission measurements are performed by heating the Ni photonic crystal to ca. 450 °C in a reductive atmosphere (5 % H_2 in Ar); the thermal emission is collected by the FTIR microscope. Emissivity is obtained by normalizing the emission from the Ni samples to that from the reference blackbody, a carbon black coated silicon wafer heated to the same temperature under Ar (Fig. 4a). Emissivity from samples of different structural openness, ranging from 26 to 5 % Ni by volume as before, is plotted together with reflectivity. Only data taken from the red color area is presented; data from the other two color areas show similar effects. Spectra are grouped in pairs: each pair of the same gray level belongs to the same structural openness. Emissivity appears as a mirror image of reflectivity ($\varepsilon = 1 - R$) even down to fine details for all wavelengths above 2 μm, confirming that the emission from the metal photonic crystal is modulated in a similar fashion as the reflectance. For

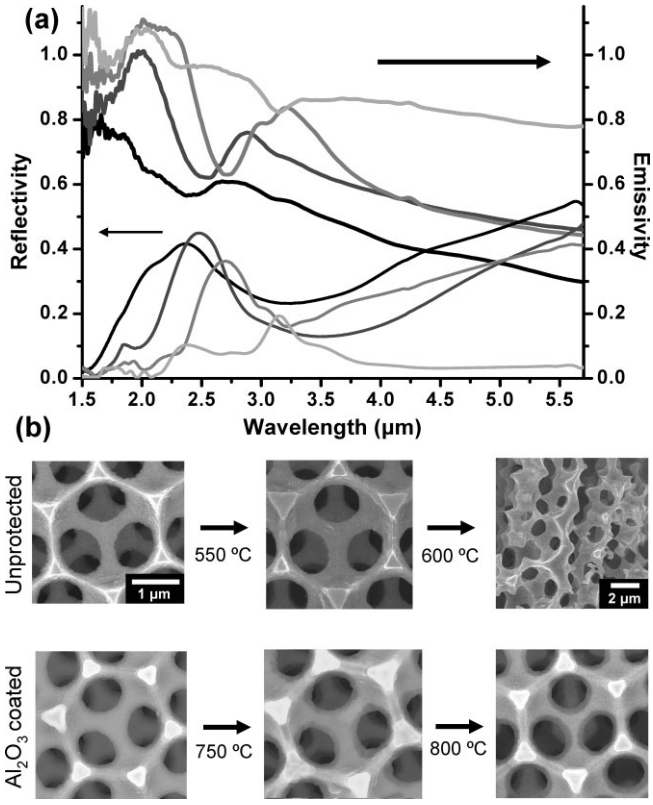

Figure 4. Emission and thermal stability of a Ni inverse opal. a) Reflectivity and emissivity measured from the red topography area of Ni inverse opals are plotted together. Samples heated to ca. 450 °C for emission studies. See text for details. Each pair of lines of the same gray scale are taken from the same spot of a sample at the same FF. FFs correspond to those presented in Figure 2. Thick lines (emissivity) closely match one minus the thin lines (reflectivity), as expected. b) Top-view SEM images of Ni inverse opal after heat treatment at various temperatures. The top row is an unprotected structure, the bottom row an Al_2O_3 protected nickel structure. Images are taken after holding the sample at the indicated temperature for 1 h under a reductive atmosphere. All images are the same magnification except for the top right image, which is presented at a lower magnification as indicated to more clearly show the structural collapse.

wavelengths below 2 μm, the relationship disappears as Bragg scattered light is not collected, leading to an underestimation of the reflectivity. Emissivity in some cases slightly exceeds one, almost certainly because the surface temperature of Ni samples is slightly higher than that of the reference sample; a temperature difference of ca. 5 °C is sufficient to explain this result. The emission of the carbon black sample is greater, and thus it is slightly cooler than the metal inverse opals, even though the temperature of the substrate heater is the same for both experiments. The metallic inverse opal does not appear to suppress thermal emission as efficiently as has been observed in lithographically fabricated metallic photonic crystals.[2]

A Ni inverse opal can be heated to ca. 550 °C without structural degradation. However, once heated to 600 °C, it significantly collapses, even under a reductive atmosphere (Fig. 4b).

ADVANCED MATERIALS

For thermal emission applications, it may be desirable for the metal structure to survive at higher temperature, for example, at 700 °C, blackbody emission peaks near 3 μm. To protect the inverse opal structure, a 50 nm thick layer of Al_2O_3 is coated on the sample via atomic layer deposition. No change is observed in reflectivity or SEM images before and after the sample is held at 750 °C for 1 h under a reductive atmosphere, the same treatment at 800 °C results in only slight changes, indicating the Al_2O_3 layer increases the working temperature of the Ni structure by at least 200 °C.

In conclusion, these experiments demonstrate that high-quality 3D metallic photonic-crystal structures can be made through a combination of colloidal-crystal templated electrodeposition and electropolishing. Only after the structure is considerably opened up, allowing light to penetrate deep into the structure, do 3D optical properties appear. Emission is indeed strongly modified by the photonic crystal. Because our experiments probe all possible degrees of structural openness and surface topographies, we can conclusively measure the maximum possible modulation of the emission along the <111> directions for an face centered cubic inverse opal structure. Although this modulation may not be sufficient for some applications, the electrochemical infilling and etching approach described here is quite flexible and is compatible with other methods commonly used to generate 3D photonic crystals, including laser holography,[19] direct writing,[20] and phase mask lithography.[21] It is likely that a combination of these methods can generate structures with narrow emissive features.

Experimental

The substrate was prepared by evaporating ca. 30 nm of gold on a 700 μm thick silicon wafer using 1 nm of chromium as an adhesion layer. It was then soaked in a saturated 3-mercapto-1-propanesulfonic acid, sodium salt ($HS\text{-}(CH_2)_3\text{-}SO_3Na$) ethanol solution for 30 min forming a monolayer of hydrophilic molecules on the gold surface. 2.2 μm diameter sulfate-terminated PS spheres (Molecular Probes) were formed into an opal film on this substrate via evaporative deposition at 50 °C with a colloid volume concentration of 0.4 % in water [22]. Ni was electrodeposited using the electrodeposition solution Techni Nickel S (Technic) under constant current mode (1 mA cm^{-2}) in a two-electrode setup with a platinum flag as the anode. Electropolishing was performed using the solution, EPS1250 (Electro Polish Systems) under constant voltage mode (4 V) in a two-electrode setup with a stainless-steel plate as cathode. Polishing was performed with 1 s pulses with 10 s intervals. The interval was selected to allow ions to diffuse in and out of the inverse opal between etching pulses. Optical measurements were carried out on a Bruker vertex 70 FTIR coupled with a Hyperion 1000 microscope. A CaF_2 objective (2.4X, NA = 0.07) was used for all measurements. A Linkam THMS600 heating chamber with a KBr window was used to heat the sample. Gas flow was regulated at 2 L min^{-} in all measurements. The substrate heater was set at 500 °C for all emission experiments. Due to thermal resistance of the substrate, the surface temperature of the substrate was about 50 °C lower than that of the substrate heater. Temperature survivability studies were performed in a tube furnace (Lindberg Blue M) under a flowing reductive atmosphere (5 % H_2 in Ar).

Received: December 6, 2006
Published online: June 1, 2007

[1] W. Y. Zhang, X. Y. Lei, Z. L. Wang, D. G. Zheng, W. Y. Tam, C. T. Chan, P. Sheng, *Phys. Rev. Lett.* **2000**, *84*, 2853.
[2] J. G. Fleming, S. Y. Lin, I. El-Kady, R. Biswas, K. M. Ho, *Nature* **2002**, *417*, 52.
[3] S. Y. Lin, J. Moreno, J. G. Fleming, *Appl. Phys. Lett.* **2003**, *83*, 380.
[4] E. Ozbay, *Science* **2006**, *311*, 189.
[5] I. Puscasu, M. Pralle, M. McNeal, J. Daly, A. Greenwald, E. Johnson, R. Biswas, C. G. Ding, *J. Appl. Phys.* **2005**, *98*, 013 531.
[6] M. I. Baraton, L. Merhari, *Synth. React. Inorg. Met.-Org. Chem.* **2005**, *35*, 733.
[7] J. Banhart, *Prog. Mater. Sci.* **2001**, *46*, 559.
[8] A. L. Pokrovsky, V. Kamaev, C. Y. Li, Z. V. Vardeny, A. L. Efros, D. A. Kurdyukov, V. G. Golubev, *Phys. Rev. B* **2005**, *71*, 165 114.
[9] W. J. Li, G. Sun, F. Q. Tang, W. Y. Tam, J. S. Li, C. T. Chan, P. Sheng, *J. Phys. Condens. Matter* **2005**, *17*, 2177.
[10] G. von Freymann, S. John, M. Schulz-Dobrick, E. Vekris, N. Tetreault, S. Wong, V. Kitaev, G. A. Ozin, *Appl. Phys. Lett.* **2004**, *84*, 224.
[11] P. N. Bartlett, M. A. Ghanem, I. S. El Hallag, P. de Groot, A. Zhukov, *J. Mater. Chem.* **2003**, *13*, 2596.
[12] B. H. Juarez, C. Lopez, C. Alonso, *J. Phys. Chem. B* **2004**, *108*, 16 708.
[13] P. N. Bartlett, J. J. Baumberg, S. Coyle, M. E. Abdelsalam, *Faraday Discuss.* **2004**, *125*, 117.
[14] P. N. Bartlett, P. R. Birkin, M. A. Ghanem, *Chem. Commun.* **2000**, 1671.
[15] T. A. Kelf, Y. Sugawara, J. J. Baumberg, M. Abdelsalam, P. N. Bartlett, *Phys. Rev. Lett.* **2005**, *95*, 116 802.
[16] R. M. Cole, Y. Sugawara, J. J. Baumberg, S. Mahajan, M. Abdelsalam, P. N. Bartlett, *Phys. Rev. Lett.* **2006**, *97*.
[17] T. W. Ebbesen, H. J. Lezec, H. F. Ghaemi, T. Thio, P. A. Wolff, *Nature* **1998**, *391*, 667.
[18] D. L. C. Chan, M. Soljacic, J. D. Joannopoulos, *Phys. Rev. E: Stat. Phys., Plasmas, Fluids, Relat. Interdiscip. Top.* **2006**, *74*, 016 609.
[19] M. J. Escuti, G. P. Crawford, *Opt. Eng.* **2004**, *43*, 1973.
[20] G. M. Gratson, M. J. Xu, J. A. Lewis, *Nature* **2004**, *428*, 386.
[21] S. Jeon, J. U. Park, R. Cirelli, S. Yang, C. E. Heitzman, P. V. Braun, P. J. A. Kenis, J. A. Rogers, *Proc. Natl. Acad. Sci. USA* **2004**, *101*, 12 428.
[22] V. L. Colvin, *MRS Bull.* **2001**, *26*, 637.

